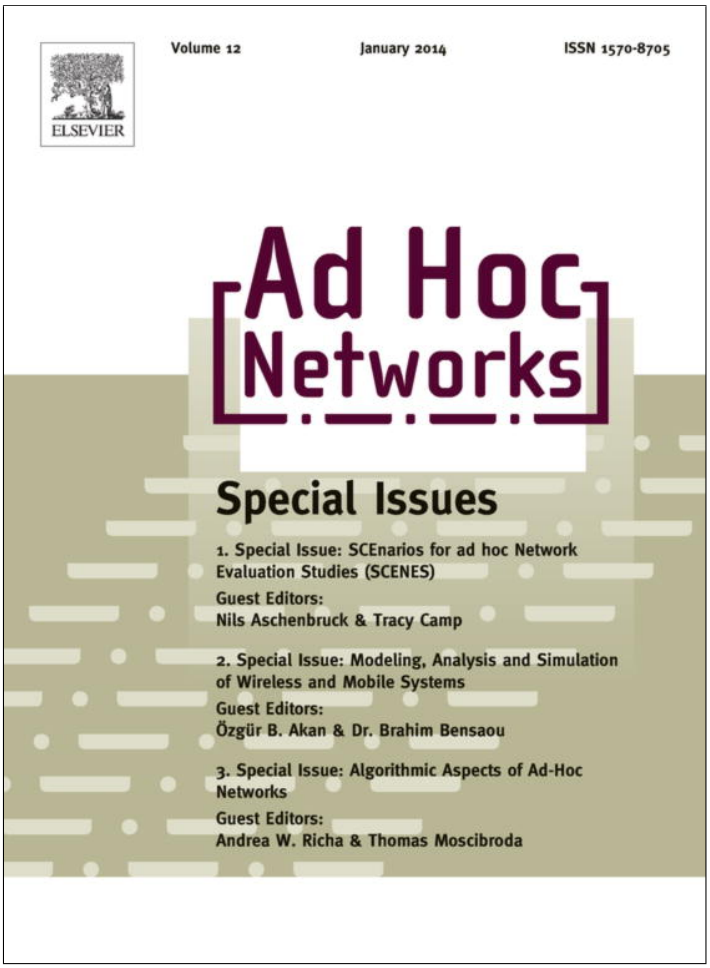

Ad Hoc Networks 12 (2014) 150–164

Contents lists available at SciVerse ScienceDirect

Ad Hoc Networks

journal homepage: www.elsevier.com/locate/adhoc

Capacity scaling in free-space-optical mobile ad hoc networks

Mehmet Bilgi *, Murat Yuksel

University of Nevada, Reno, CSE Department, MS 171, 1664 N. Virginia Street, Reno, NV 89557, USA

ARTICLE INFO

Article history:
Available online 20 December 2011

Keywords:
Free-space-optics
Mobile ad hoc networks
Angular diversity
Spatial reuse
Directional communication
Spherical FSO structures

ABSTRACT

Wireless networking has conventionally been realized via radio-frequency-based communication technologies. Free-space-optical (FSO) communication with an innovative multi-element node design leverages spatially-diverse optical wireless links; making it a viable solution to the well-known diminishing per-node throughput problem in large-scale RF networks. Although it has the advantage of high-speed modulation, maintenance of line-of-sight between two FSO transceivers during a transmission is a challenge since FSO transmitters are highly directional. In this paper, we present our simulation efforts to make high-level assessments on throughput characteristics of FSO-MANETs while considering properties of FSO propagation and existence of multiple directional transceivers. We identify the intermittent connectivity problem that is caused by the relative mobility of nodes with multiple directional transceivers. We propose two cross-layer buffering schemes to remedy this problem and present their performance results. We conclude that sophisticated buffering mechanisms are required to properly buffer a packet during the misalignment period of two communicating nodes to avoid negative effects of this intermittency on the transport layer.

1. Introduction

The capacity gap[1] between RF wireless and optical fiber (wired) network speeds remains huge because of the limited availability of the RF spectrum [1]. Though efforts for an all-optical Internet [2–4] will likely provide cost-effective solutions to the last-mile problem within the *wireline* context, high-speed Internet availability for mobile ad hoc nodes is still mainly driven by the RF spectrum saturations and spectral efficiency gains through innovative multi-hop techniques such as hierarchical cooperative MIMO [5]. To achieve high-speed wireless point-to-point communications, free-space-optical (FSO) communication has received attention particularly for high-altitudes such as space communications [6] and building-top metro-area communications [7,8]. Main focus of these efforts has been on reaching *long* (i.e., ~km) communication distances with *highly expensive* FSO components (e.g., lasers) using highly sensitive mechanical steering technologies to remedy vibration or swaying issues. In parallel to these, another common deployment scenario is interconnects made of expensive and sensitive materials. Similarly, they deal with misalignment issues caused by vibration [9,10].

An FSO transceiver is a pair of optical transmitter (e.g., Light Emitting Diode (LED)) and optical receiver (e.g., Photo-Detector (PD)). Such optoelectronic transceivers are cheap, small, low weight, amenable to dense integration (1000 + transceivers possible in 1 sq. ft), very long lived/reliable (10 years lifetime), consume low power (100 mW for 10–100 Mbps), can be modulated at high speeds (1 GHz for LEDs/VCSELs and higher for lasers), offer highly directional beams for spatial reuse and security, and operate in large swathes of unlicensed spectrum amenable to wavelength-division multiplexing (infrared/visible). To counteract these numerous advantages, FSO requires clear

* Corresponding author. Tel.: +1 7752292593.
E-mail addresses: mbilgi@cse.unr.edu (M. Bilgi), yuksem@cse.unr.edu (M. Yuksel).
URLs: http://www.cse.unr.edu/~mbilgi/ (M. Bilgi), http://www.cse.unr.edu/~yuksem/ (M. Yuksel).

[1] Part of this manuscript has been previously published in SPIE '10, LANMAN '10, and MSWiM '10 conferences.

1570-8705/$ - see front matter © 2011 Published by Elsevier B.V.
doi:10.1016/j.adhoc.2011.12.003

line-of-sight (LOS) and LOS alignment. FSO communication also suffers from beam spread with distance (tradeoff between per-channel bit-rate and power) and unreliability during bad weather especially when size of particles in the medium are close to the used wavelength (aerosols and fog).

Recent work [11–17] showed that FSO mobile ad hoc networks (FSO-MANETs) are possible by means of "optical antennas", i.e., FSO spherical structures like those shown in Fig. 1. This figure exhibits a sample wireless optical antenna design with hexagonal faces. Each face contains multiple FSO transceivers and each face can be tailored to maintain connection with a neighbor. This hexagonal antenna design introduces the "group of transceivers" concept on each face in comparison to uniform spherical design. A group of transceivers can transmit exactly the same signal to increase coverage in expense of some reduced spatial reuse and provide benefits in managing per-flow buffers. Such FSO spherical structures (i) achieve *angular diversity* via spherical surface, (ii) achieve *spatial reuse* via directional optical transmitters, and (iii) are *multi-element* since they are covered with multiple transceivers.

FSO communication can be used in indoor and outdoor settings, where existing lighting infrastructure can also be leveraged for communication purposes. For example, in a traffic setting, where accident information must be delivered to the cars in the same road, FSO can be used to deliver this information using traffic lights as well as cars' lights in a multi-hop manner. Similarly, traffic lights can be used to serve commercial audio or video content. Furthermore, exit lights inside the buildings can communicate with the hand held devices of disaster victims to direct them to the nearest safe exit as well as to localize them for aftermath rescue [18].

In this paper, we examine a subset of the research problems brought by using such multi-element FSO structures in MANETs and proposals to remedy such issues. We specifically investigate the issues raised by directionality in combination with mobility and their implications on TCP and overall network throughput. We present a thorough simulation study that covers all the important system parameters. Our previous work [16] showed that using multi-transceiver FSO nodes to establish a general-purpose communication method is possible via a proof-of-concept prototype made of off-the-shelf optoelectronic components. In this paper, we extend the study to MANET scenarios involving many of such multi-transceiver nodes, and investigate achievable throughput gains in comparison to a pure RF-based MANET. Our contributions include:

- Quantification of negative effects of multi-element FSO structures on end-to-end throughput.
- Modules to realistically simulate FSO nodes in NS-2 with consideration of crucial parameters such as visibility, divergence angle, line-of-sight, alignment, and obstacles.
- A quantitative analysis of overall performance of FSO networks and their comparison to similarly designed RF networks.
- Proposals for solving the intermittent connectivity problem for multi-transceiver FSO nodes and their implications on overall network throughput.

The rest of the paper is organized as follows: In Sections 2 and 3, we give the literature background information for FSO networks and the theoretical model for optical propagation in free space, respectively. In Section 4, we discuss the details of our contribution to NS-2 to accurately simulate networks of multi-element FSO nodes. In Section 5, we illustrate the observed throughput change while altering mobility, visibility and divergence angle in the system. We also look at the density of nodes in the network and its implications on throughput. Later, we focus on specific use cases of FSO in which there are obstacles: a city environment and a lounge setup and compare the results with RF. In Section 6, we propose two buffering mechanisms and provide throughput results to assess their effectiveness. We discuss our conclusions and future work in Section 7.

2. Background

Majority of the current deployments of FSO communications is targeted at long distance point-to-point applications: terrestrial last-mile, deep space [6] and building-top installations, where redundancy or limited spatial reuse is achieved through one primary beam and some backup beams. Building-top installations employ high speed modulation of laser, that is generated by expensive and highly sensitive equipment [7,8] to expand the transmission range and overcome the challenges of propagation medium (especially fog and aerosols). This kind of FSO deployment is typically a mesh network installation in which FSO links establish the backbone of the network, because of their high throughput capacity. Eliminating the need to lay cable, especially in geographically challenging environments is the main motivation of building-top and last-mile point-to-point FSO deployments. Various techniques have been developed for such stationary deployments of FSO

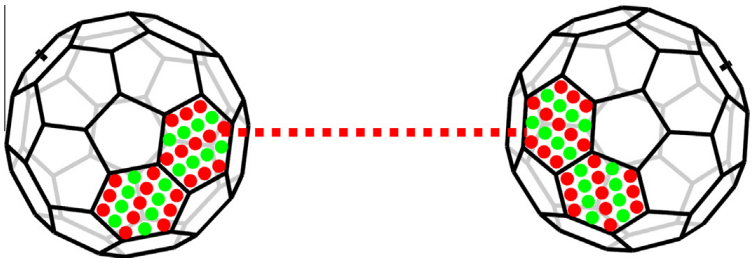

Fig. 1. Two "soccer-ball-shaped" optical antennas, accommodating an array of transceivers mounted on each hexagon, are communicating with each other.

to tolerate small vibrations [19], swaying of the buildings and scintillation, using mechanical auto-tracking [20–22] or beam steering [23], where the main focus was on small vibrations or swaying *but node mobility was not even considered possible*.

Employment of FSO communication in indoor environments has been done mainly by using diffuse optics [24–26]. Such proposals have been challenged due to limited power of a single source that is being diffused in all directions. Also quasi-diffuse techniques use multiple transmitters (still with very large angles) to overcome the sensed power problem. Since they rely on the reflected signals in a bounded propagation medium (e.g., in a small room), they have limited range (10 s of meters) and are not suitable for outdoor use.

The idea of using multiple elements/transceivers in FSO communication has been used in interconnects [9,27–29], which communicate over very short distances (e.g., cms) within a computer rack or case. The main issues of such multi-element operation are interference (or cross-talk) between adjacent transceivers due to finite divergence of the light beam and misalignment due to vibration. Multi-element operation has been suggested not only for increasing the capacity of the overall system, but also for achieving robustness due to spatial diversity in the case of misalignment. Our work considers multi-element FSO designs as a general-purpose communication technology working over distances much longer than the interconnects.

Leveraging of multiple directional transceivers in RF-based MANETs was also considered recently. Similar to our electronic steering among FSO transceivers to track line-of-sight alignment, authors of[30] dynamically optimized the best way of selecting a stationary access point and directional RF antenna on a moving vehicle in a seamless manner. In the same vein, several link layer techniques [31,32] used directional RF antennas to improve wireless multicast throughput. The trade-off between wireless beam directionality and diversity has been an attractive research topic [33], and our work mainly targets establishing building blocks to explore this key trade-off in FSO networking.

3. FSO Propagation model

We used well-known FSO propagation models [23] to simulate power attenuation characteristics of an FSO signal. LED's light intensity profile follows the Lambertian law [23], i.e., intensity is directly proportional to the cosine of the angle from which it is viewed. At a distance Z, let the received power along the beam be P_Z. Based on the Lambertian law, at an arbitrary angle α from the vertical axis and at a distance Z, the intensity would be: $P_{\alpha,Z} = P_Z\, cos(\alpha)$. For edge-emitting LEDs, this is improved by a factor u in the power of cosine, i.e., the intensity is given by: $P_{\alpha,Z} = P_Z \cos^u(\alpha)$.

Also, as a generic definition for all FSO transmitters, the beam radius w_Z at the vertical distance Z is defined as the radial distance at which the received power is $\frac{1}{e^2} P_Z$. Hence, the divergence angle θ is the special value of α, where the ratio $P_{\alpha,Z}/P_Z = 1/e^2$ holds, which means θ can be calculated by $\theta = tan^{-1}(w_Z/Z)$.

FSO propagation is affected by both the atmospheric attenuation A_L and the geometric spread A_G, which practically necessitates the source power to be greater than the power lost. The *geometric attenuation* A_G is a function of transmitter radius γ, the radius of the receiver on the other receiving FSO node ς cm, divergence angle of the transmitter θ and the distance between the transmitting node and receiving node R:

$$A_G = 10 \log \left(\frac{\varsigma}{\gamma + 200R\theta} \right)^2$$

The *atmospheric attenuation* A_L consists of absorption andscattering of the light photons by different aerosols and gaseous molecules in the atmosphere. The power loss due to atmospheric propagation is given by Bragg's Law [23] as:

$$A_L = 10 \log(e^{-\sigma R})$$

where σ is the attenuation coefficient consisting of atmospheric absorption and scattering. For the wavelengths used for FSO communication, Mie scattering dominates the other losses, and therefore is given by [34]:

$$\sigma = \frac{3.91}{V} \left(\frac{\lambda}{550} \right)^{-q}.$$

In the above formulation of σ, V is the atmospheric visibility in kilometers, q is the size distribution of the scattering particles whose value is dependent on the visibility:

$$q = \begin{cases} 1.6 & V \geqslant 50 \text{ km} \\ 1.3 & 6 \text{ km} \leqslant V < 50 \text{ km} \\ 0.583V^{1/3} & V < 6 \text{ km} \end{cases}$$

4. Multi-transceiver FSO nodes

To accurately quantify the throughput characteristics of FSO-MANETs, we developed extensions to the well-known network simulator NS-2 [35]. A necessary extension item was to enable multiple transceivers in a wireless mobile node to transmit and receive data simultaneously. For this purpose, we duplicated the stack elements that belong to physical and link layers. Fig. 2 shows our mobile node architecture in NS-2 simulator. Traditional mobile node design contains only one network stack which contains link layer, interface queue, MAC, and wireless phy objects. A packet handed from application layer to the routing agent would travel from link layer object all the way down to wireless phy and reach the wireless channel. In our modified implementation of a wireless node, routing agent is capable of handling multiple interfaces, and hence, has multiple network stacks corresponding to each optical transceiver on the node. Depending on the aligned target interfaces of an antenna, the routing agent selects the appropriate link layer object to hand the packet to. This modification essentially required us to change the routing agent and necessary routing table constructs to make routing agent aware of multiple physical interfaces. Moreover, we introduced an alignment list structure for each of these interfaces to keep track of the alignment states of each

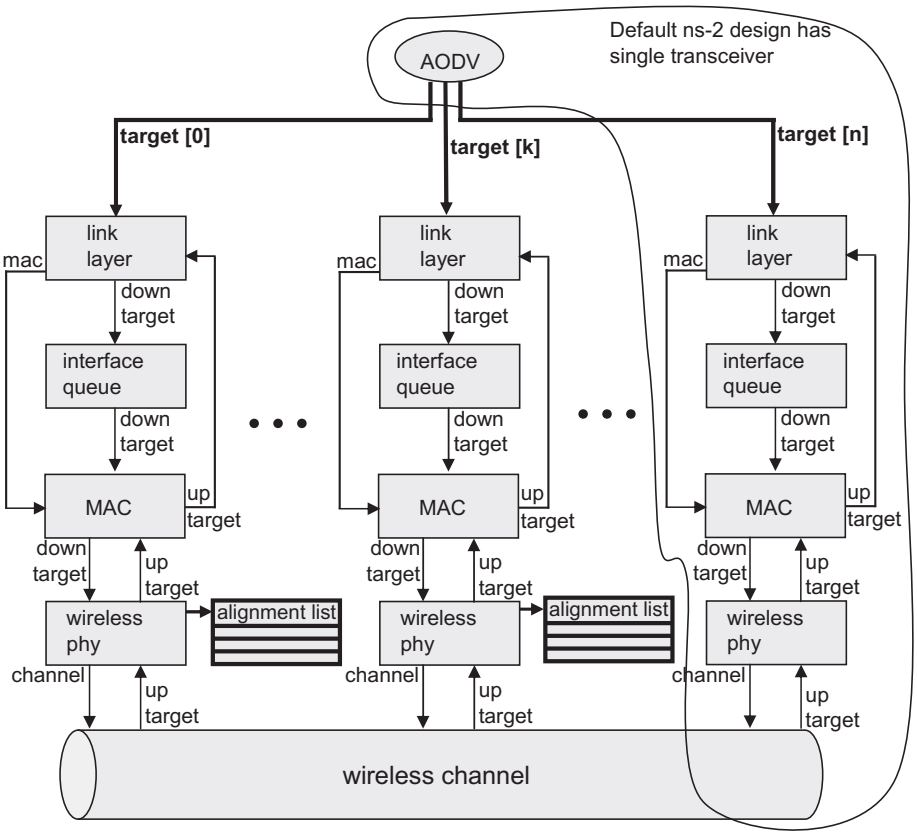

Fig. 2. FSO node structure with a separate stack for each optical transceiver.

transceiver. The alignment list of a transceiver contains information revealing the identifiers of currently aligned target transceivers (Fig. 3). Physical channel implementation is also modified so that only the candidate recipients in the alignment lists are considered to determine if a successful transmission of a packet is achievable. In this section, we discuss our contributions to NS-2 to make assessments on FSO-MANETs' throughput characteristics.

4.1. Wireless mobile node modifications

We used AODV in our simulations as the routing agent. The routing agents available in NS-2 that can be used in mobile wireless nodes assume there is only one interface. We modified this behavior and made AODV capable of handling multiple interfaces. For each interface, there exists a complete set of stack objects from AODV down to physical channel (Fig. 2).

This model of dedicating a separate stack for each transceiver enables the wireless mobile node's MAC interfaces to conduct the medium access control responsibilities asynchronously from each other. That is, since there are n MAC objects in total for n transceivers, there can be n *simultaneous* flows to different nodes. This is essential to our simulation effort since it enables us to exploit *spatial reuse* of the physical medium in FSO communication. As a future direction, we would like to unify those n stacks into one using a directional MAC which can essentially cope with n simultaneous flows through n transceivers but takes its packets from only one queue object. We expect to see increased responsiveness to mobility since it is aware of the directional nature of the underlying communication channel.

4.2. LOS re-alignment mechanism

In a multi-transceiver wireless mobile node setting, a node has to keep track of its aligned transceivers. Instead of more traditional methods like mechanical steering, we use electronic LOS tracking and management, i.e., *electronic*

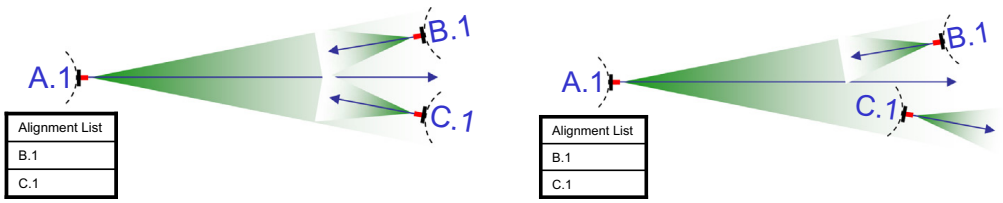

(a) A.1 has bi-directional alignment with both B.1 and C.1 (b) A.1 has lost alignment with C.1

Fig. 3. Possible scenario of two communicating transceivers loosing their alignment with each other.

steering. We use a fairly straightforward alignment re-establishment protocol. A transceiver periodically sends out search (SYN) frames to find out if a link can be established. If a neighbor node's transceiver receives such a search frame, it responds accordingly with a SYN_ACK frame. Finally, an ACK frame completes a 3-way handshake which ensures that the alignment is mutual, that is, both transceivers are in line-of-sight with each other.

This periodic re-establishment of alignments has implications on the delivery process of a packet. Routing agent assumes that each interface has multiple wireless physical links to different nodes and it places packets accordingly in the appropriate queue. As soon as MAC discovers an opportunity to send out a packet, it takes a packet from the queue and forwards it to channel object after an RTS/CTS exchange. At this point, channel checks if the next hop is in the alignment list of the sending transceiver (Fig. 2). Moreover, if the next hop is in the alignment list, channel checks once more to determine if the two interfaces are still aligned. Note that the role of the alignment list is sufficiently exerted by the first check. Channel implementation is being conservative by conducting the second check, since, although the next hop node is in the alignment list of the sender, it may have gained mobility and lost its line-of-sight.

Table 1
Table of default values common to each simulation set in validation simulations.

Parameter name	Default value
Visibility	6 km
Number of interfaces	8
Transmission range and separation between nodes	30 m
Divergence angle	1 rad
Photo detector diameter	5 cm
LED diameter	0.5 cm
Per-bit error probability	10^{-6}
Noise	1.1428e−12 W
Capture threshold	1.559e−11 W
Receive threshold	3.652e−10 W

Finally, our LOS establishment and tracking mechanism conservatively assumes that links are bi-directional. It is possible to extend our LOS re-alignment algorithm such that unidirectional links can be established. Such a uni-directional alignment model would increase the spatial reuse and the effective throughput by leveraging scenarios, where forward and reverse transmission channels go over different transceivers and/or multiple hops. For instance, node A can send to node B via its transceiver 1 while node B can respond to node A's transceiver 3 back via node C. Such optimizations are quite possible in stationary or low-mobility settings, and it will require a MAC protocol customized for this directional multi-transceiver environment.

4.3. Characterization of a single-hop FSO link

After introducing necessary mechanisms to simulate multi-element FSO nodes, we validated [15] the single hop FSO link that it conforms to the well-known FSO propagation models [23]. We observed received power, error probability, and bit error rate in packet transmissions while varying important parameters like separation between the two transceivers, visibility and noise. The set of parameters that we use in the validation simulations and their corresponding values are provided in Table 1.

4.3.1. Effect of separation

Complying with the theoretical framework, our results reveal that the received power follows Lambert's law [23] from the transmitter itself and normal of the transmitter as depicted in Fig. 4a. The original transmission power for this scenario is calculated for 0.1 m. We increased the separation between transmitter and receiver antennas from 0.01 m to 100 m in our simulations (Fig. 4a). Fig. 4b shows the Gaussian distribution of the received light intensity clearly as the receiver is moved away from transmitter's normal line by focusing on the last 10 m of Fig. 4a.

Distance also affects the theoretical error probability and simulated packet error since the received power decreases significantly. We sampled the theoretical error with separation between antennas ranging from 10 m to

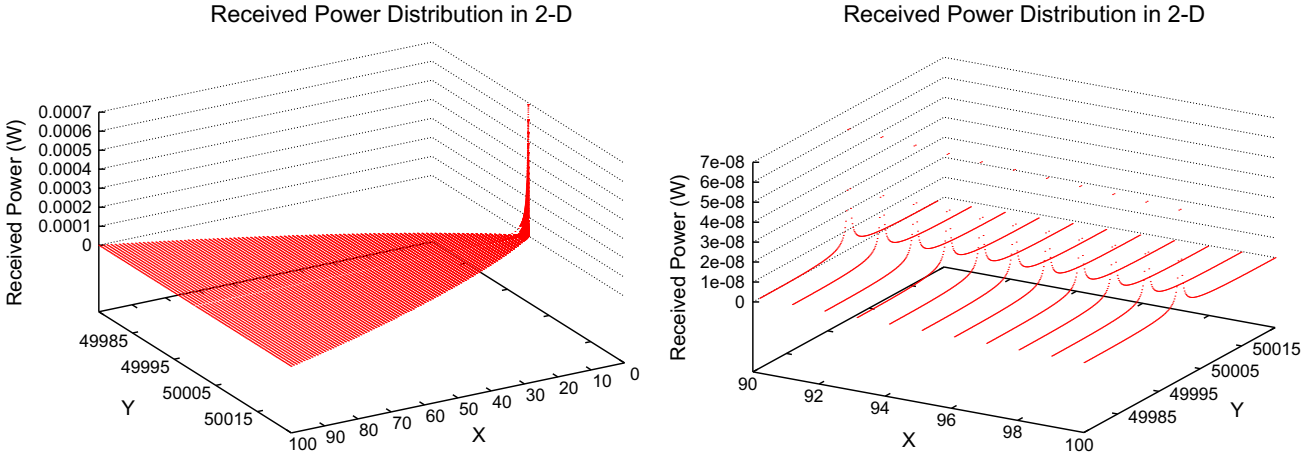

(a) Received power in the field of view of a 1 rad light source.

(b) Received power between 90 and 100 meter ranges.

Fig. 4. Distance versus received power intensity.

4000 m. Fig. 5b shows that the theoretical error probability increases significantly as the receiver is moved away from the transmitter while keeping the transmission power fixed. Similarly, the simulated packet error shown in Fig. 5a, follows the theoretical error probability.

4.3.2. Effect of visibility

Low visibility in the medium makes the light experience more deviation from its intended direction by hitting aerosols in the air. This causes the received light intensity to drop which in turn causes more bit errors. Hence, increasing visibility decreases the theoretical error probability and the simulated packet error. For this simulation scenario, the power is calculated for 100 m with 6 km visibility and kept the same for all the simulations. Separation between antennas is 100 m. We increased visibility from 0.037 km to 0.041275 km. In Fig. 6a, we show that the visibility in the medium affects the theoretical bit error probability and the simulated packet error significantly. From the figure, we can see that if visibility is set to a value from 0 to 0.037 km, the system experiences a high level of error but recovers after 0.04 km.

4.3.3. Effect of noise and interference

We found that noise has an important impact on theoretical bit error probability and simulated packet error since it is harder for the receiver to operate at a low signal-to-noise ratio. We used a transmission power that reaches 100 m with a noise level of 1.1428e−12 W for all of our simulations in this scenario. We increased the noise in the medium from 3.0e−5 W to 2.01e−4 W and found that both the theoretical error probability and simulated packet error are increased considerably as depicted in Fig. 6b.

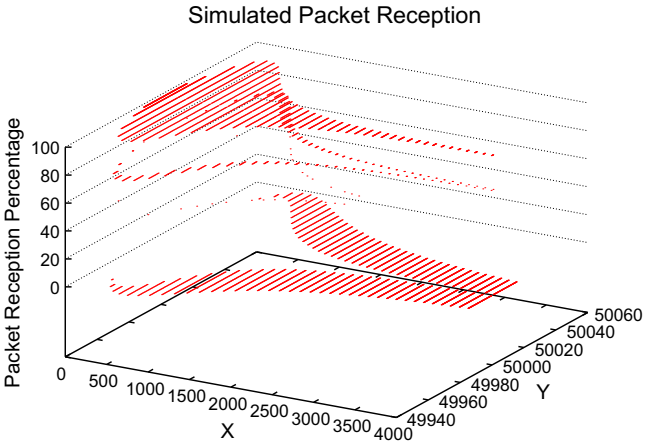

(a) Percentage of successfully delivered packets versus separation.

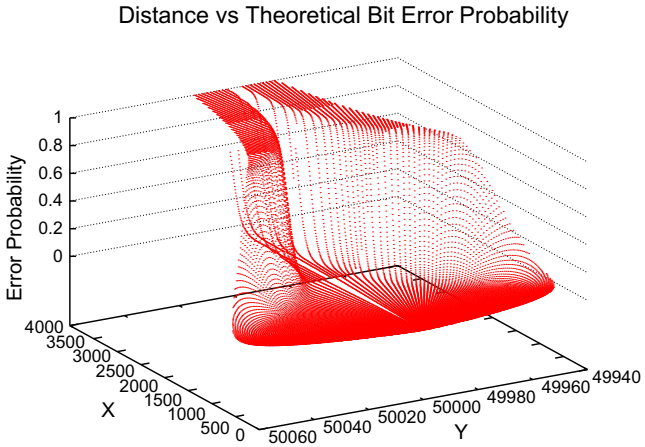

(b) Probability of error increases as a receiver is moved away from the transmitter.

Fig. 5. Distance versus packet and bit error.

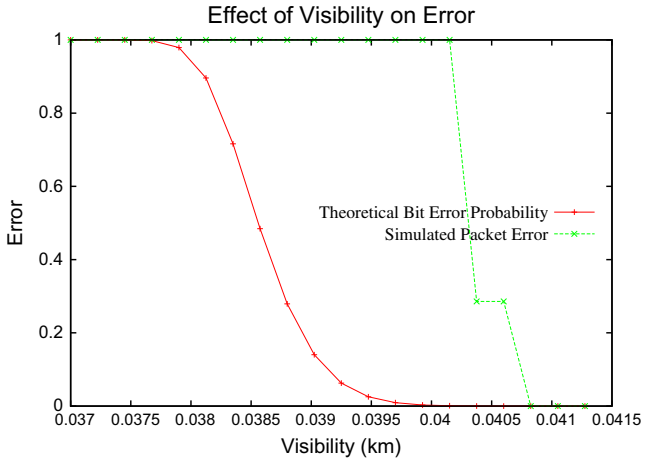

(a) Probability of error decreases as the visibility in the medium is increased.

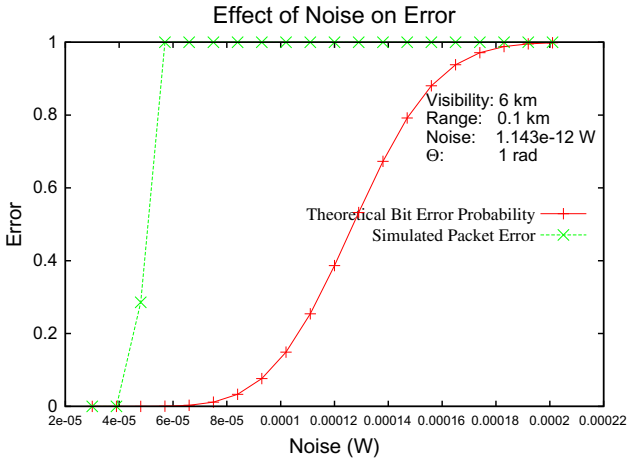

(b) Theoretical error probability with respect to noise and interference.

Fig. 6. Error probability versus visibility and noise.

5. Capacity scaling in FSO-MANETs

We perform extensive simulation experiments to investigate end-to-end throughput performance over a FSO-MANET using multi-element spherical FSO nodes. We compare FSO performance to RF under the same conditions. Particularly, we aim to answer the following research questions:

- How robust can the multi-element spherical FSO nodes be against *mobility*?
- How important are the effects of node design (e.g., number of transceivers per node) and transceiver characteristics (e.g., divergence angle) on the throughput?
- Can the FSO nodes deliver acceptable throughput in a typical *indoor* environment?
- Can the FSO nodes deliver acceptable throughput in an *outdoor* city environment, where several obstacles exist?

5.1. Simulation environment setup

Our simulations consist of 49 nodes (each with eight transceivers) organized as a 7 by 7 grid initially before they start moving. Every node opens FTP file transfer sessions on top of TCP to every other node in the network, which makes 49×48 flows in total. All the nodes are mobile doing 1 meter per second except the lounge simulations in Section 5.7, where nodes are stationary. We used an area of 210×210 m and visibility of the medium was 6 km. We ran the simulations for 3000 s and repeated each simulation for five iterations. We show the average throughput plots with 95% confidence intervals.

Table 2 shows the *default* parameters we feed to our simulation experiments. The FSO node structures are circular in shape, except the lounge scenario in Section 5.7, where the nodes are shaped as a sphere. The transceivers are placed on the nodal shape with a deterministic separation, i.e., the distance among any two neighbor transceivers is the same. The node structure has a radius of 20 cm. LEDs are 0.5 cm and PDs are 5 cm in radius.

Table 2
Table of default parameter values common to each simulation set in throughput simulations.

Parameter name	Default value
Number of nodes	49
Number of flows	49×48
Visibility	6 km
Number of interfaces	8
Mobility	1 m/s
Simulation time	3000 s
Transmission range and separation between nodes	30 m
Area	210 m by 210 m
Node radius	20 cm
Divergence angle	0.5 rad
Photo detector diameter	5 cm
LED diameter	0.5 cm

5.2. Visibility

FSO communication has been known for its intolerance to adverse weather. Especially fog has been considered as a serious threat to the reliability of the communication in traditional point-to-point applications of FSO. To quantify how aerosols affect the overall network throughput, we simulated our network scenarios under different visibility conditions. We varied the visibility in the medium from 2 m to 0.2 km. We depict our findings in Fig. 7a which shows the clear trend of increasing throughput as the visibility conditions become better.

5.3. Divergence angle

We investigated how divergence angle of transceivers affects the network throughput as well. We used different number of transceivers with varying divergence angles. Number of transceivers change from 4 up to 20 and we increase the divergence angle from 0.1 radian to 1.1 radians. Only different parameter in this scenario from the default setup given in Table 1 is that the mobility of the nodes is 0.01 m/s. One must note that, as we increase the divergence angle of transceivers, coverage area of a node starts to resemble to RF. When we increase the divergence angle of transmit and receive apparatus of antennas, we see that a transmission can be detected by a wider number of neighbor receivers in the vicinity of the transmitter. If the divergence angle is further increased, adjacent beams on a node start to overlap and cause crosstalk and interference. As a result, a given transmission is subject to a larger number of interfering transmissions. Hence, the throughput decreases as we increase the divergence angle of transceivers. This is why we see a decrease in the overall network throughput in Fig. 7b.

5.4. Mobility

A rather intriguing question is how FSO-MANETs would perform in a mobile setting. We investigate the extent of packet drops caused by mobility and compare FSO-MANETs with similarly designed RF-based networks. To answer this question, we simulated a network of FSO nodes with four transceivers, each with 1 radian of divergence angle and other networks of FSO nodes with 8 and 16 transceivers with further decreasing divergence angles. Fig. 8a shows the results of these experiments. The first observation is that while RF stays almost the same with respect to mobility, FSO throughput decreases dramatically due to the directional nature of the transceivers. Second, at low mobility rates, node designs with more transceivers achieve better throughput due to greater spatial reuse. Moreover, node designs with more transceivers and narrower angles tend to get affected more seriously from mobility. We conclude that 4-transceiver design performs the best at high mobility rates since it is the closest one to RF in terms of coverage and wide field of view. From the given results, we conclude that networks of multi-transceiver directional FSO nodes exhibit the pattern of *intermittent connectivity*. This event of frequent alignment/misalignment of the communicating transceivers af-

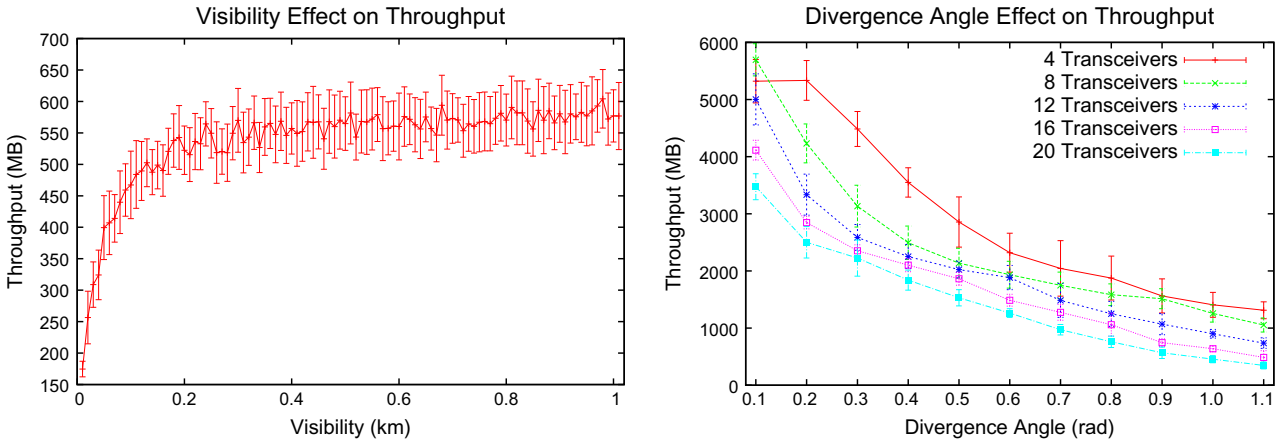

(a) Visibility Effect. (b) Divergence Angle Effect.

Fig. 7. Aggregate throughput results for different simulation scenarios.

fects TCP seriously. A solution to this problem is to introduce buffers to reduce packet drops in the event of a misalignment. Such buffering techniques can be cross-layer in that they should be able to mitigate the loss of layer 2 frames by storing them in layer 2 and/or layer 3 buffer (s) that are either shared by all the transceivers of the node or each one dedicated to different layer 3 flows.

5.5. Node density

One of the main motivations behind our work is the reduction in per-node throughput of RF-based MANETs when the network experiences a large increase in the number of actively communicating nodes. RF per-node throughput scales with $\sqrt{n}$ as number of nodes (n) grows [36] since RF spectrum becomes saturated and interference dominates the throughput behavior because of the omnidirectional RF propagation. Hence, we conducted node density experiments in which we increase the number of nodes from 10 to 150 in a confined area of 50×50 m.

First, we increase the number of nodes in the area while keeping area size and the other parameters (e.g., transmission range is 8 m (refer to the discussion in Section 4.3 for power degradation behavior)) the same. Figs. 8b and 9a show the overall network throughput and per-node throughput. We conclude that the drop in RF throughput is much more significant than the drop in FSO throughput in both scenarios, again, because of spatial reuse and decreased interference.

Second, we increase the area size and keep the number of nodes and all the other parameters (e.g., transmission range is 30 m) the same. Fig. 9b shows the network throughput as one edge of the area is increasing. The network throughput first increases as the node density is decreasing. This shows that the initial node density is too high for the 30 m transmission range and there is a significant interference. Later, as the node density gets even smaller, the network throughput starts to decrease as 30 m becomes insufficient to cover the average node separation.

5.6. Re-alignment timer

We conducted another set of simulations to find out the effect of re-alignment timer on throughput and failure. We repeated the experiments for 20 iterations with different random seeds and we depicted 95% confidence intervals. In Fig. 10, we show how overall network throughput and failure are affected with this phenomenon. Our conclusion is that especially the failures are not dramatically affected with larger timer intervals which is an important finding to reduce the re-alignment overhead.

5.7. Obstacle scenarios in lounge and city environments

We extended our simulation effort to find out how FSO behaves in possible applications in indoor and outdoor environments. For indoor, we considered a lounge setting, where there is a dense presence of nodes on top of tables that are 10 m apart from each other. We placed either 2 or 4 spherical nodes on 16 tables which makes 48 nodes each with 18 transceivers. We placed access point FSO nodes with 26 transceivers at arbitrary locations shown in Fig. 11b including one in a second floor, where all the FTP traffic is to and from this node through nine access points. Similarly, Fig. 11a shows upper left quarter of the network establishing FTP sessions to and from node 10 through access point 1 The remaining quarters of the network have similar FTP sessions with their corresponding remote nodes, where traffic needs to be relayed by an access point node. We observe a significant difference in throughput as shown in Fig. 10a in lounge settings due to the difference in propagation nature of RF and FSO.

For outdoor, we put 25 (in a 5 by 5 setting) buildings with 10 m of separation from each other. Between each building, there are two people and 1 car. Our re-alignment algorithm takes the obstacles into account so that if a building is blocking two communicating devices, they have to find other intermediate nodes that will carry their traffic. We also modified the default NS-2 random way-point

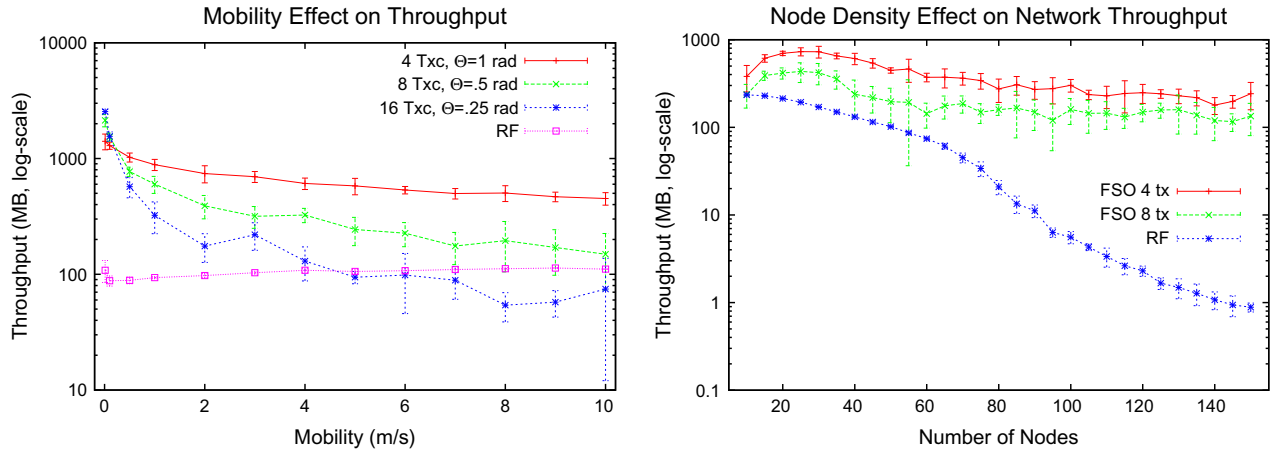

(a) Mobility Effect.

(b) Network-wide throughput.

Fig. 8. Aggregate throughput results for different simulation scenarios.

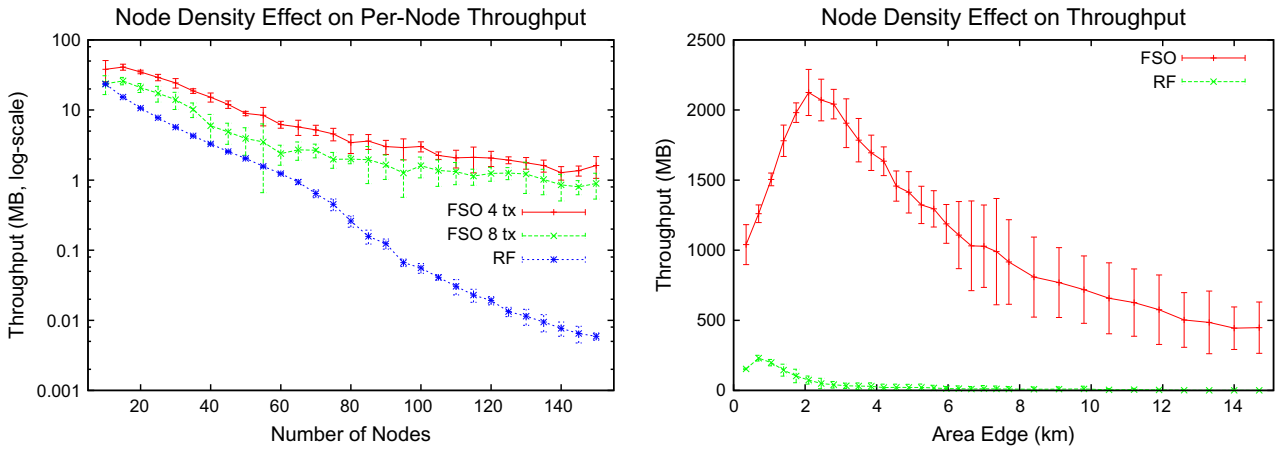

(a) Per-node throughput.

(b) Enlarging Simulation Area.

Fig. 9. Aggregate throughput results for different simulation scenarios.

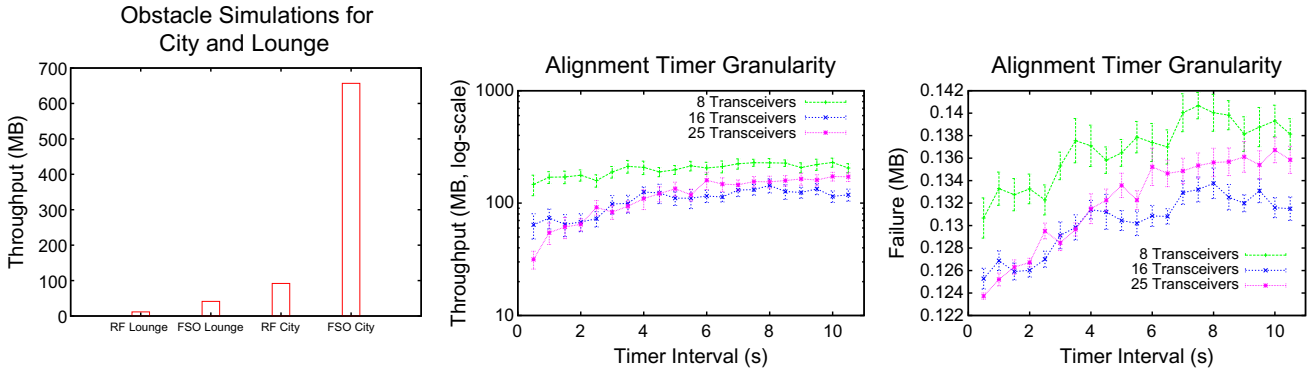

(a) Throughput comparisons for in-door and out-door deployment of RF and FSO.

(b) Alignment timer effect on throughput in log-scale.

(c) Alignment timer effect on throughput.

Fig. 10. Obstacle and alignment timer simulation results.

mobility generator to acknowledge existing obstacles. We did not penalize RF transmissions going through those obstacles since RF signal can get through obstacles although the signal strength drops in reality. Observe that

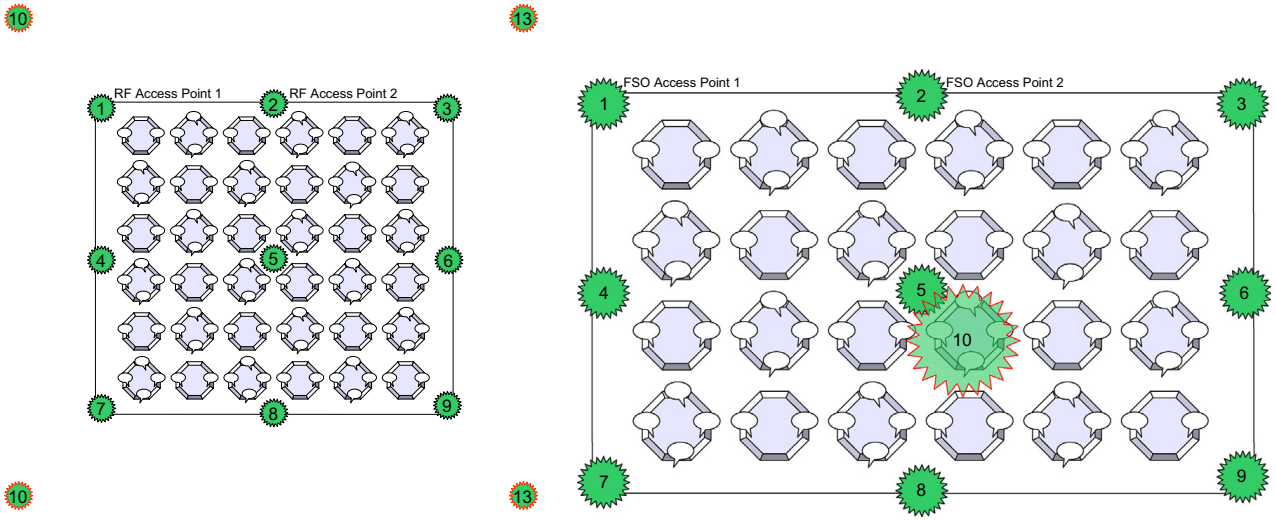

(a) A dense lounge setting with multiple RF wireless devices to demonstrate the substantially decreasing per node throughput problem in RF.

(b) A two story lounge with FSO nodes communicating with another backend node in the second floor.

Fig. 11. Placement of FSO and RF nodes in a lounge environment.

FSO's spatial reuse makes a significant difference compared to RF simulation result even though this is an outdoor scenario (Fig. 10a). Note that we observe such results since obstacles are blocking the communication only temporarily because of mobility of the nodes.

6. Buffering techniques against intermittent connectivity

Section 5 revealed an important phenomenon, i.e., high intermittent connectivity, that emerges only when a large number highly-directional transceivers are used at each node in a mobile wireless network. The intermittent connectivity patterns arising from highly directional transceivers need special treatment, since existing networking protocols and technologies are designed with the assumption that there exists an underlying link that is always connected. Such an issue does not emerge in today's wireless networks, where a few (typically 3–5) directional RF antennas are used for each coverage cell [37]. To the best of our knowledge, the intermittent connectivity pattern is currently specific to multi-transceiver free-space-optical mobile ad hoc networks since directional RF antennas generate much larger communication lobes [37]. However, we envision that as directional RF antennas become more precise and more focused with smaller divergence angles, researchers will experience similar problems in bridging the gap between existing protocols and an underlying communication paradigm, where connectivity is highly intermittent. Additionally, we anticipate that, as the boundaries between delay-tolerant networking (DTN) and conventional networks disappear, buffering techniques relevant in DTN area will be introduced for similar buffer management issues, especially considering directional communication possibility for DTNs because of power consumption benefits.

In this section, we propose two buffering schemes: *node-wide* and *per-flow* buffering to achieve better throughput in mobile settings, where intermittence of the underlying wireless links is the norm. The common point to both of these buffering schemes is that they keep an otherwise-would-be-dropped packet during the misalignment period of two communicating nodes till an alignment is re-established through the same or a different pair of transceivers. We discuss the aforementioned buffering schemes in Sections 6.1 and 6.2 in detail and provide differences in their behavior. We give the performance results of major simulation settings and compare the two buffering mechanisms with non-buffered performance results in this section.

6.1. Node-wide buffering

Algorithm 1. Node-wide Buffering

```
1: DEFINE LINK LAYER ROUTINE:
2: UPON Reception Of Packets At Link Layer:
3: if This interface is aligned with the next hop of the
   packet then
4:       Enqueue the packet in the interface queue
5: else
6:       DISPATCH the packet
7: end if
8: DEFINE REALIGNMENT HANDLER ROUTINE:
9: UPON The Event Of Realignment:
10: for all Interfaces of the node do
11:      for all Packets in the interface queue do
12:           if The interface is not aligned with the
   next hop of the packet then
13:                DISPATCH the packet
14:           end if
15:      end for
```

(continued on next page)

```
16: end for
17: for all Packets in the node-wide buffer do
18:     for all Interfaces of the node do
19:         if The interface became aligned with the
    next hop of the packet then
20:             Deliver the packet to the
    corresponding link layer
21:         end if
22:     end for
23: end for
24: DEFINE DISPATCH ROUTINE:
25: for all Interfaces of the node do
26:     if The interface is aligned with the next hop of
    the packet then
27:         Deliver the packet to the
    corresponding link layer
28:         EXIT ROUTINE
29:     end if
30: end for
31: BUFFER the packet
32: DEFINE BUFFER ROUTINE:
33: if Node-wide buffer is full then
34:     Drop the packet
35: else
36:     Put packet at the end of the buffer
37: end if
```

Node-wide buffering mechanism, whose algorithm is given in Algorithm 1, uses a single buffer for all the transceivers in the node. This buffer is a simple drop-tail memory space that holds packets if the next hop of the packet is not aligned.

Consider a packet going through the layers of the node stack depicted in Fig. 2. First, the routing agent (i.e., AODV) will select the outgoing interface to the best of its knowledge. Since the routing agent operates at a much coarser time scale than realignment periods, it is possible that the alignment to the next hop node no longer exists when the packet is handed from the routing agent to the queue of the interface. Upon reception of a packet, the queue checks the alignment list of the interface to see if the next hop of the packet is still aligned. If the next hop is aligned, the packet gets queued at that outgoing interface. If the next hop is not aligned, the packet will be handed to a dispatching function to see if any of the interfaces of the node are aligned with the next hop. If an appropriate interface is found, the packet will be delivered to the correct link layer object. If no interface is found, the packet will be buffered in the node-wide buffer. If the node-wide buffer is already at its full capacity, then the packet will be dropped.

In the event of realignment, we go through all the queues in the node and try to place the packets to the correct outgoing queue. If the packet's next hop is not aligned through any transceiver, the packet is put to node-wide buffer. Additionally, we also consider each packet in the buffer and try to deliver it to the appropriate link layer object if one of the interfaces become aligned with the next hop of a packet in the buffer.

6.2. Per-flow buffering

Algorithm 2. Per-flow Buffering

```
1: DEFINE LINK LAYER ROUTINE:
2: UPON Reception Of Packets At Link Layer:
3: BUFFER the packet according to its next hop address
4: if MAC is idle then
5:     FETCH a packet for this interface and deliver it
    to MAC
6: end if
7: DEFINE FETCH ROUTINE:
8: for all Per-flow buffers in the node do
9:     if Buffer's next hop node is aligned with this
    interface then
10:         Place the buffer at the end of the node's
    list of per-flow buffers
11:         RETURN a packet from the buffer
12:     end if
13: end for
14: DEFINE IDLE MAC HANDLER ROUTINE:
15: UPON MAC becoming idle:
16: FETCH a packet for this interface and deliver it to
    MAC
17: DEFINE BUFFER ROUTINE:
18: if Buffer space is full then
19:     Drop the packet
20: else
21:     for all Per-flow buffers in the node do
22:         if Buffer's next hop and packet's next hop
    are the same then
23:             Place the packet into the buffer
24:             EXIT ROUTINE
25:         end if
26:     end for
27:     Create a new buffer
28:     Place the packet into the buffer
29: end if
```

In the per-flow buffering mechanism, we keep a buffer for each next hop node as explained in Algorithm 2. After the routing agent hands the packet to the link layer, queue forwards the packet to a per-flow buffer according to the next hop address field of the packet. It does not check if this interface is aligned with the next hop of the packet or not. The interface then explicitly checks if the MAC is idle. If the MAC state is idle, the interface retrieves a packet to its queue from one of the buffers whose next hop is aligned with this interface and that packet is handed to the MAC.

Additionally, whenever the MAC becomes idle again, it notifies the interface about its idle state and that again causes the interface to retrieve a packet to its queue from one of the per-flow buffers whose next hop nodes are known to be aligned with this interface. We time-stamp the packet retrieval times from each per-flow buffer. When MAC requests a packet, we have a number of per-flow buffers to retrieve a packet from, considering that the interface is aligned with multiple nodes. Among those candidate per-flow buffers, we select the one that has the

Table 3
Abbreviations for quantities of buffering components.

Quantity	Abbreviation
Number of buffers	n
Number of interfaces	k
Max node-wide buffer size	t
Queue size	q
Max per-flow buffer size	p

Table 4
Complexity of each major step in buffering.

Action	Node-wide buffer	Per-flow buffer
Enqueue	k (Redirection)	n (Packet checkout)
Buffer	Constant	n (Find target buffer)
Queue resume	Constant	n
Realignment	$k^*q + t$ (Deliver the queues and buffer)	Not applicable
Fathom timer	Not applicable	n^*p

oldest packet retrieval time. By doing so, we ensure that all of the flows experience a more fair scheduling. Note that we dedicate buffers according to the next hop address of the packets, not the destination address. Also, we acknowledge that the original behavior of the FIFO queue is no longer preserved since packets belonging to the same flow will be queued based on their arrival but packets from different flows will be multiplexed while being sent out.

Table 4 provides the complexity of each step involved in the transmission process of a packet. With the help of Table 3, we see that per-flow buffering scheme's computational complexity can easily hinder its responsiveness and agility when it has a large number of next-hop neighbors, and thus per-flow buffers. A typical example of this is when the nodes are moving with a low mobility and hence, have a larger number of per-flow buffers.

Finally, we implemented a timer mechanism to discard the packets in stale buffers. Such a timer makes room for the new flows by periodically discarding all the packets in a buffer if it has not been accessed during the last timer period. Since the timer period is as long as multiple realignment intervals, discarding stale buffers is safe because the next hop is declared unreachable after multiple realignment trials.

6.3. Buffering performance results

After implementing all the necessary buffering extensions for both schemes, we re-ran major simulation scenarios that we have discussed in Section 5. To lay out the simulation setup: we had 49 nodes with eight transceivers. Each transceiver had a divergence angle of 0.5 rad. The default mobility of the nodes is 1 m/s and transmission range and the node separation is 30 m. Nodes move according to a random way point algorithm in an area of 210 m by 210 m. In each simulation set, we modify a default parameter and observe its effect on overall network throughput.

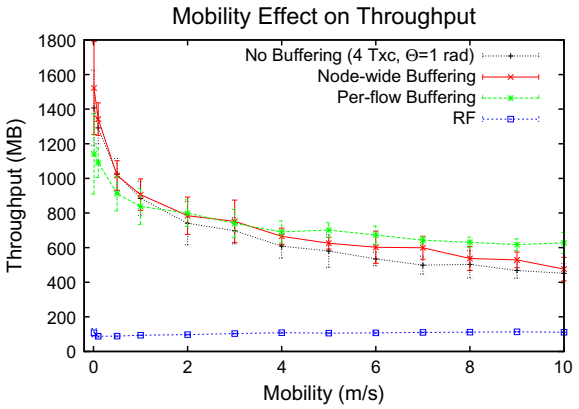

Fig. 12. Throughput results for four transceiver node design.

We repeat each simulation five times and plot with 95% confidence intervals.

The most important of the simulations is the mobility simulation set which have a critical role in judging the effectiveness of our approach since our aim is to enable high mobility in FSO-MANETs via these buffering schemes. We have considered three node designs for mobility scenarios. In Figs. 12 and 13a and b, we show the results in a network that consists of FSO nodes with 4, 8, and 16 interfaces, respectively. We gradually increase the average speed of each node in the network and plot the overall network throughput. We observed that the per-flow buffering performs poorly compared to non-buffered case and node-wide buffering at low speeds due to the overhead caused by per-flow buffering and its implications on other layers. Moreover, at high speeds and at nodes with larger number of transceivers, per-flow buffering scheme out-performs node-wide buffering due to its much more fine-grained scheduling of the packets and larger buffer space.

Fig. 13b clearly shows that the per-flow buffering mechanism is superior to both the node-wide and non-buffered cases. Both node-wide buffering and default no buffering approaches deteriorate under the RF throughput line at high speeds while per-flow mechanism steadily provides better results. We conclude that even though our graphs suggest using the node-wide buffering approach for low mobility, per-flow buffering provides the best possible results for high-speed settings and node designs with large number of transceivers.

The second important set of simulations is node density scenarios. We have previously concluded that per-node RF throughput reaches its limit as we add more nodes to the network. We have also shown that FSO performs much better due its spatial reuse in Section 5. In Fig. 14a and b, we provide the results for the overall network throughput and per-node throughput for a network of FSO nodes with four transceivers. We also show the eight transceiver case in Fig. 15a and b. In all of these four graphs, we see a constant increase in overall network throughput when either of the two buffering mechanisms is used. Additionally, per-flow buffering provides better throughput results compared to node-wide buffering and this fact is depicted more clearly when we increase the number of transceivers. In Fig. 16a, we depict the results of a scenario, where the

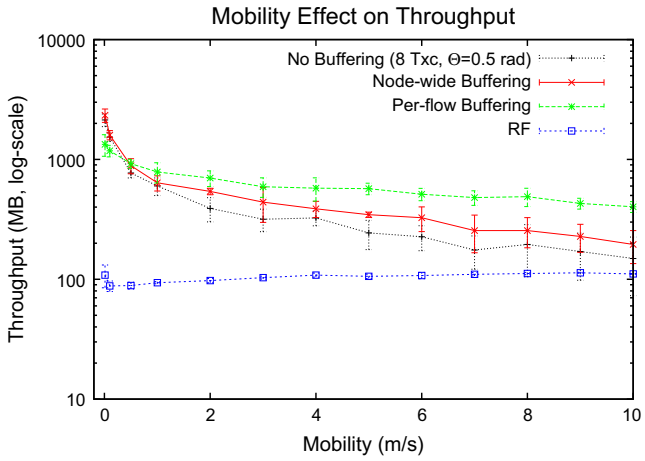

(a) Mobility results for 8 transceiver node design.

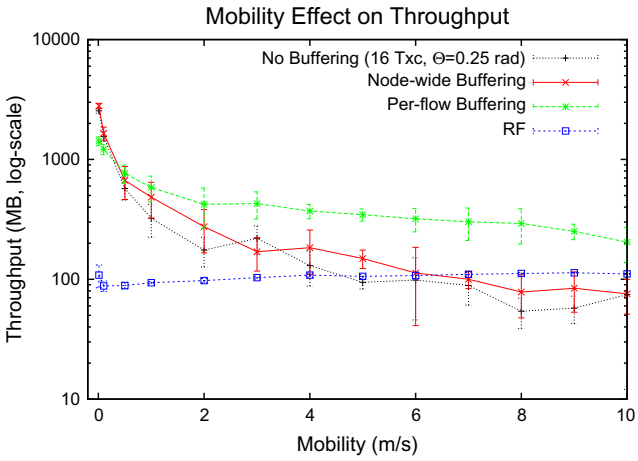

(b) Mobility results for 16 transceiver node design.

Fig. 13. Throughput results for 8 and 16 transceiver node designs.

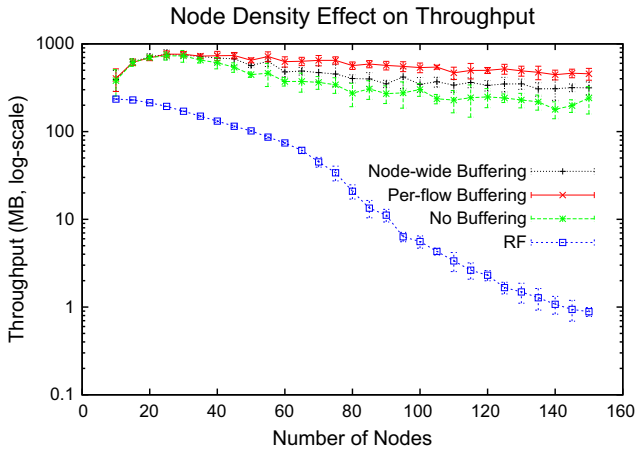

(a) Node density results in which the number of nodes are increased (4 transceivers).

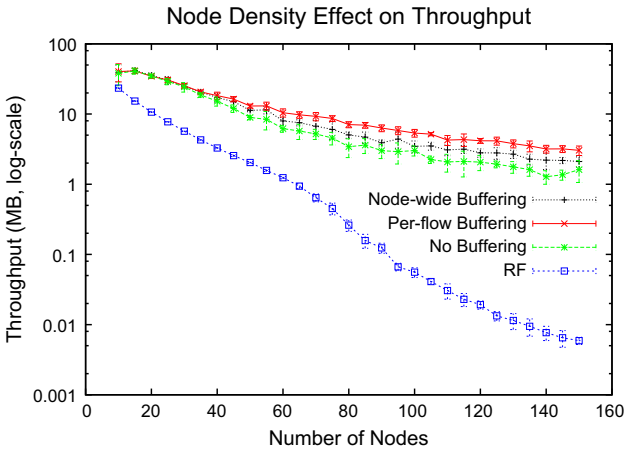

(b) Node density results showing per-node throughput (4 transceivers).

Fig. 14. Throughput results for node density simulations.

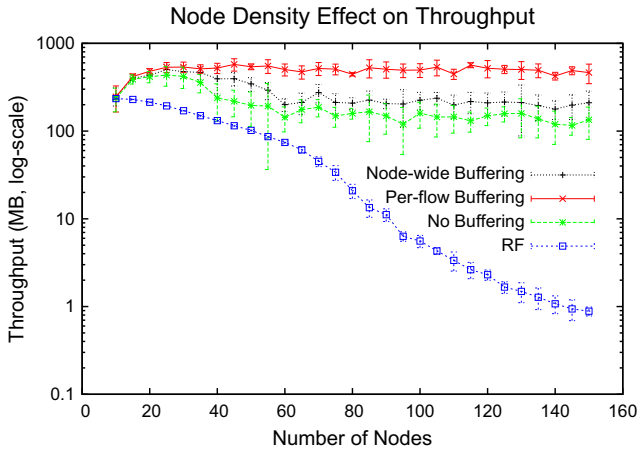

(a) Node density results in which the number of nodes are increased (8 transceivers).

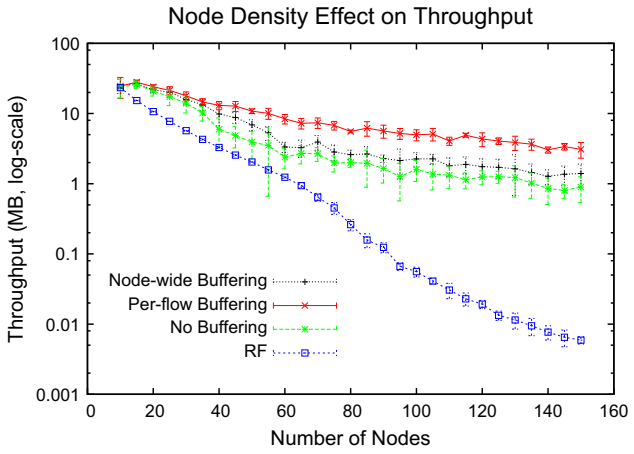

(b) Node density results showing per-node throughput (8 transceivers).

Fig. 15. Throughput results for node density simulations.

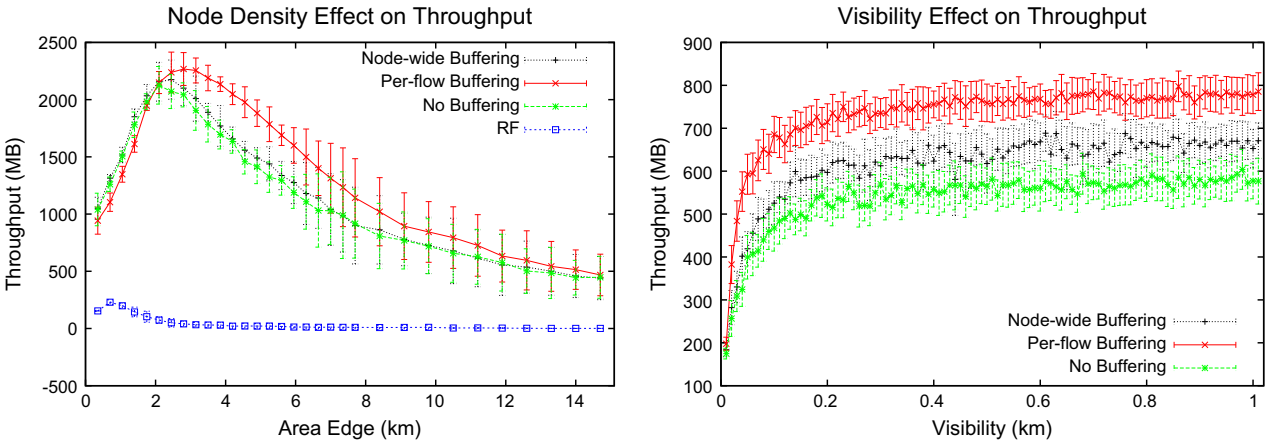

(a) Node density results for fixed power and enlarged area configuration.

(b) Visibility simulations.

Fig. 16. Throughput results for node density and visibility simulations.

transmission power of the transceivers are kept the same and the area is made larger. We observe that, at first the area was very small for the network, and as we make the area larger, the overall throughput increases. After the peak point, the throughput starts to drop due to insufficient power and reduced coverage. Here, we observe in Figs. 14a and b, 15a and b and 16a that with buffering, the difference between RF and FSO per-node end to end throughput enlarges.

Additionally, we show that the visibility case shows a steady increase in throughput from buffering as well (Fig. 16b). We observe that this particular speed of 1 m/s differentiates the two buffering schemes nicely and shows that per-flow outperforms the node-wide scheme once more.

7. Summary and discussion

In this paper, we presented our contribution to NS-2 network simulator, mainly on FSO propagation model, multi-transceiver directional FSO structures, and obstacle-avoiding mobility generation. We assessed the effects of multiple system parameters on the overall network throughput.

FSO-MANETs are fundamentally different than RF-based MANETs because of the highly-directional FSO communication and its implications on higher layers when it is combined with mobility. In such a realization of a network of multi-transceiver nodes equipped with a large number highly directional transceivers, we see that a pattern of intermittency emerges due to relative mobility of communicating nodes. This phenomena is clearly non-existent in omni-directional RF networks since the physical link preserves its characteristics for a long time. Changes to the channel quality are rare and hence, transport level protocols run smoothly. However, FSO's intermittent connectivity causes degradation in link quality in significantly smaller time scales and severely affects TCP.

We conclude that our simulations of FSO networks deployed in lounge and downtown city environments show clear advantage over RF deployments. We have provided details of two buffering schemes to remedy the problem of reduced throughput in multi-transceiver free-space-optical mobile ad hoc networks due to high intermittence of the optical wireless link. We discussed their design in detail and identified their differences. We have provided their throughput results for increasing mobility and number of transceivers. We conclude that the per-flow buffering provides better network-wide throughput than the node-wide buffering mechanism. We leave scheduling fairness and buffer allocation issues as future work. We observe that more rigorous theoretical modeling of achievable capacity with multi-transceiver spherical nodes can be made. However, since such an effort deserves a paper by itself, we left the comparison of our approach to the existing FSO modeling efforts in a theoretical framework [38] to a future study.

Acknowledgment

This work is supported in part by NSF awards 0721452 and 0721612.

References

[1] C. Davis, Z. Haas, S. Milner, On how to circumvent the MANET scalability curse, in: Proceedings of IEEE MILCOM.
[2] A.R. Moral, P. Bonenfant, M. Krishnaswamy, The optical internet: architectures and protocols for the global infrastructure of tomorrow, IEEE Communications Magazine 39 (2001) 152–159.
[3] D.K. Hunter, I. Andonovic, Approaches to optical internet packet switching, IEEE Communications Magazine 38 (2000) 116–122.
[4] M. Yoo, C. Qiao, S. Dixit, Optical burst switching for service differentiation in the next-generation optical internet, IEEE Communications Magazine 39 (2001) 98–104.
[5] A. Ozgur, O. Levesque, D. Tse, Hierarchical cooperation achieves optimal capacity scaling in ad hoc networks, IEEE Transactions on Information Theory 53 (2007) 3549–3572.
[6] V.W.S. Chan, Optical space communications: a key building block for wide area space networks, IEEE Lasers and Electro-Optics Society 1 (1999) 41–42.
[7] Terabeam Inc., Terabeam Inc., 2000. <Http://www.terabeam.com.>
[8] Lightpointe Inc., Lightpointe Inc., 1998. <Http://www.lightpointe.com>.
[9] T. Sakano, Novel free-space optical interconnection architecture employing array devices, Electronics Letters 27 (1991) 515–516.

[10] D.J. Goodwill, Free space optical interconnect at 1.25 gb/s/channel using adaptive alignment, in: Optical Fiber Communication Conference and the International Conference on Integrated Optics and Optical Fiber Communication (OFC/IOOC), pp. 259–261.
[11] J. Akella, M. Yuksel, S. Kalyanaraman, Error analysis of multi-hop free-space-optical communication, Proceedings of IEEE International Conference on Communications (ICC) 3 (2005) 1777–1781.
[12] M. Yuksel, J. Akella, S. Kalyanaraman, P. Dutta, Free-space-optical mobile ad hoc networks: auto-configurable building blocks, ACM Springer Wireless Networks 15 (2009) 295–312.
[13] M. Bilgi, M. Yuksel, Multi-element free-space-optical spherical structures with intermittent connectivity patterns, in: Proceedings of IEEE INFOCOM Student Workshop.
[14] B. Nakhkoob, M. Bilgi, M. Yuksel, M. Hella, Multi-transceiver optical wireless spherical structures for MANETs, IEEE Journal on Selected Areas of Communications 27 (2009).
[15] M. Bilgi, M. Yuksel, Packet-based simulation for optical wireless communication, in: Proceedings of IEEE Workshop on Local and Metropolitan Area Networks, IEEE, 2010.
[16] A. Sevincer, M. Bilgi, M. Yuksel, N. Pala, Prototyping multi-transceiver free-space-optical communication structures, in: Proceedings of IEEE International Conference on Communications.
[17] W. Di, A. Alhussein, Throughput and delay analysis for hybrid radio-frequency and free-space-optical (RF/FSO) networks, Springer Wireless Networks 17 (2011) 877–892.
[18] M. Bilgi, M. Yuksel, N. Pala, 3-d Optical wireless localization, in: Proceedings of IEEE GLOBECOM 2010 Workshop on Optical Wireless Communications.
[19] S. Arnon, N.S. Kopeika, Performance limitations of free-space optical communication satellite networks due to vibrations-analog case, SPIE Optical Engineering 36 (1997) 175–182.
[20] E. Bisaillon, D.F. Brosseau, T. Yamamoto, M. Mony, E. Bernier, D. Goodwill, D.V. Plant, A.G. Kirk, Free-space optical link with spatial redundancy for misalignment tolerance, IEEE Photonics Technology Letters 14 (2002) 242–244.
[21] J.W. Armstrong, C. Yeh, K.E. Wilson, Earth-to-deep-space optical communications system with adaptive tilt and scintillation correction by use of near-earth relay mirrors, OSA Optics Letters 23 (1998) 1087–1089.
[22] M. Naruse, S. Yamamoto, M. Ishikawa, Real-time active alignment demonstration for free-space optical interconnections, IEEE Photonics Technology Letters 13 (2001) 1257–1259.
[23] H. Willebrand, B.S. Ghuman, Free Space Optics, 1st ed., Sams Publishings, 2001.
[24] D.C. O'Brien et al., High-speed integrated transceivers for optical wireless, IEEE Communications Magazine 41 (2003) 58–62.
[25] D.J.T. Heatley, D.R. Wisely, I. Neild, P. Cochrane, Optical wireless: the story so far, IEEE Communications 36 (1998) 472–474.
[26] J. Derenick, On the deployment of a hybrid FSO/RF mobile ad-hoc network, in: IEEE/RSJ International Conference on Intelligent Robots and Systems.
[27] S. Tang, R. Chen, L. Garrett, D. Gerold, M.M. Li, Design limitations of highly parallel free-space optical interconnects based on arrays of vertical cavity surface-emitting laser diodes, microlenses, and photodetectors, Journal of Lightwave Technology 12 (1994) 1971–1975.
[28] D. Tsang, H. Roussell, J. Woodhouse, J.D. ly, C. Wang, D. Spears, R. Bailey, D. Mull, K. Pedrotti, C. Seabury, High-speed high-density parallel free-space optical interconnections, in: LEOS '94 Conference Proceedings, pp. 217–218.
[29] F. Tooley, R. Morrison, S. Walker, Design issues in free-space digital optics, in: Third International Conference on Holographic Systems, Components and Applications, 1991.
[30] V. Navda, A.P. Subramanian, K. Dhanasekaran, A. Timm-Giel, S. Das, Mobisteer: using steerable beam directional antenna for vehicular network access, in: MobiSys '07: Proceedings of the 5th International Conference on Mobile Systems, Applications and Services, ACM, New York, NY, USA, 2007, pp. 192–205.
[31] S. Sen, R. Ghosh, J. Xiong, R.R. Choudhury, Poster abstract: Beamcast: harnessing beamforming capabilities for link layer multicast, SIGMOBILE Mobile Computing Communication Review 13 (2009) 34–37.
[32] K. Sundaresan, K. Ramachandran, S. Rangarajan, Optimal beam scheduling for multicasting in wireless networks, in: MobiCom '09: Proceedings of the 15th Annual International Conference on Mobile Computing and Networking, ACM, New York, NY, USA, 2009, pp. 205–216.
[33] K. Ramachandran, R. Kokku, K. Sundaresan, M. Gruteser, S. Rangarajan, R2d2: regulating beam shape and rate as directionality meets diversity, in: MobiSys '09: Proceedings of the 7th International Conference on Mobile Systems, Applications, and Services, ACM, New York, NY, USA, 2009, pp. 235–248.
[34] H.C. Van de Hulst, Light Scattering by Small Particles, John Wiley and Sons, 1957.
[35] The Network Simulator, 1995. <Http://www.isi.edu/nsnam/ns/>.
[36] P. Gupta, P. Kumar, The capacity of wireless networks, IEEE Transactions on Information Theory 46 (2000) 388–404.
[37] K. Pedersen, P. Mogensen, J. Ramiro-Moreno, Application and performance of downlink beamforming techniques in UMTS, Communications Magazine, IEEE 41 (2003) 134–143.
[38] Jing Li, Murat Uysal, Achievable information rate for outdoor free space optical communication with intensity modulation and direct detection, in: Global Telecommunications Conference, GLOBECOM '03. IEEE, 2003.

Mehmet Bilgi has received his Ph.D. from the CSE Department of The University of Nevada, Reno (UNR) in December 2010. During his studies at UNR, he has worked on simulation of multi-element free-space-optical MANETs under the supervision of Dr. Murat Yuksel. His research focused on throughput capacity of FSO-MANETs, relative localization using orientation-only methodologies, and prototyping such systems. His research interests are in the computer networks and distributed systems area in general. He received his M.S. degree from UNR in May, 2008 and B.S. degree from Computer Engineering Department of Fatih University, Istanbul, Turkey in June, 2005. He is a member of Sigma Xi, ACM, and IEEE.

Murat Yuksel is currently an Assistant Professor at the CSE Department of The University of Nevada, Reno (UNR), Reno, NV. He was with the ECSE Department of Rensselaer Polytechnic Institute (RPI), Troy, NY as a Postdoctoral Research Associate and a member of Adjunct Faculty until 2006. He received a B.S. degree from Computer Engineering Department of Ege University, Izmir, Turkey in 1996. He received M.S. and Ph.D. degrees from Computer Science Department of RPI in 1999 and 2002 respectively. His research interests are in the area of computer communication networks with a focus on protocol design, network economics, wireless routing, free-space-optical mobile ad hoc networks (FSO-MANETs), and peer-to-peer. He is a member of IEEE, ACM, Sigma Xi, and ASEE.